

Supplementary Information

Analysis of H₂O-induced surface degradation in SrCoO₃-derivatives and its impact on redox kinetics

Andrea Cavallaro,* George E. Wilson, Gwilherm Kerherve, Eleonora Cali, Celeste A. M. van den Bosch, Paul Boldrin, David Payne, Stephen J. Skinner and Ainara Aguadero.

* Corresponding author: a.cavallaro@imperial.ac.uk

Department of Materials,
Imperial College London,
London SW7 2AZ,
UK.

Figure S1

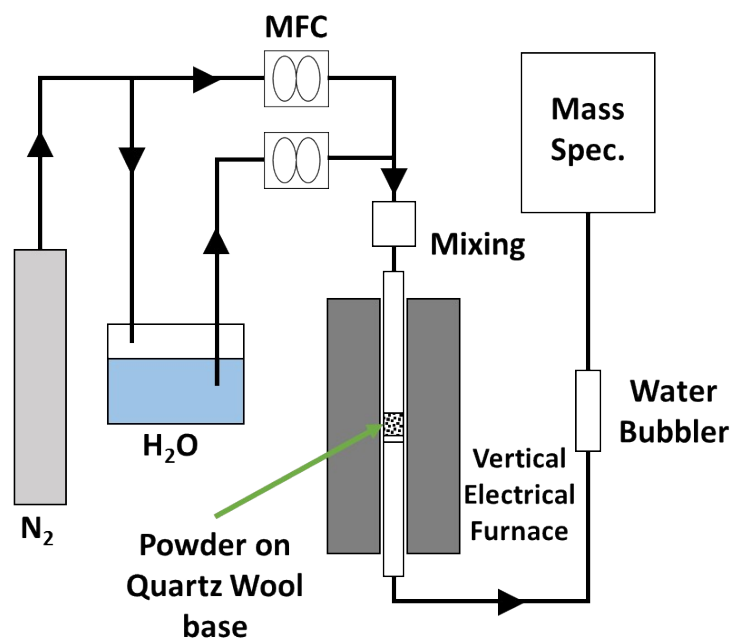


Figure S 1: Schematic of the thermochemical water splitting set-up.

Figure S2

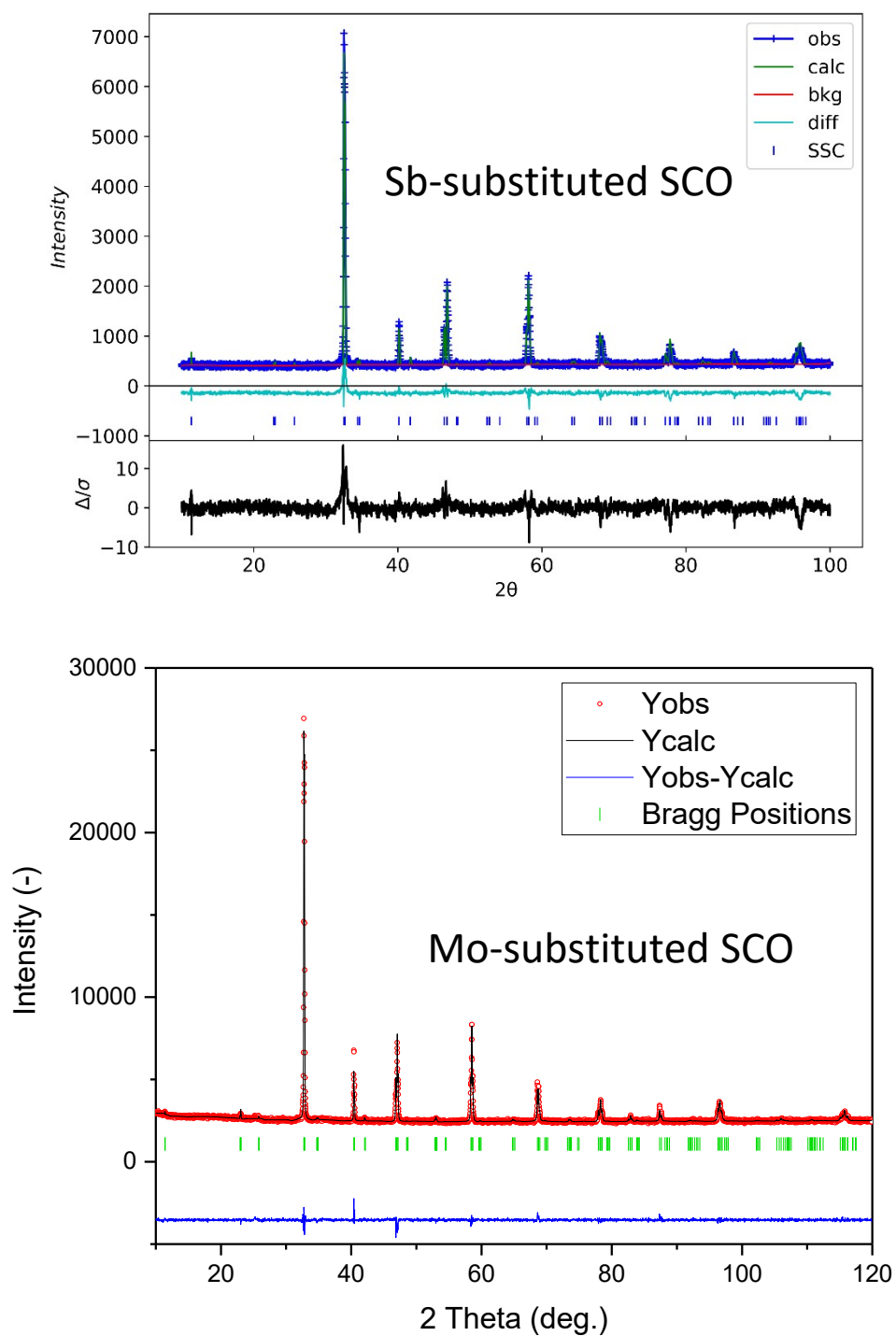


Figure S 2: XRD data Rietveld refinement of the SCS and SCM powders after the synthesis. Sb-SCO was analysed by GSAS II while Mo-SCO by FullProf software.

Figure S3

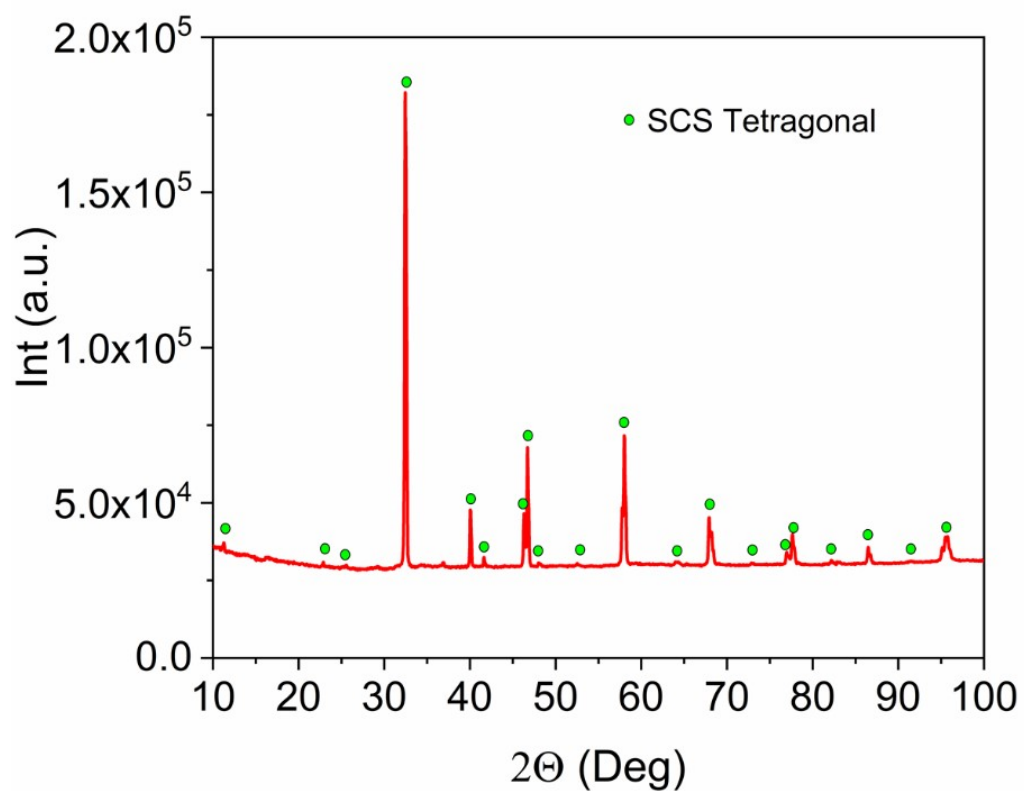


Figure S 3: XRD-analysis of SCS powder after RT water cleaning and drying process at 100 °C.

Figure S4

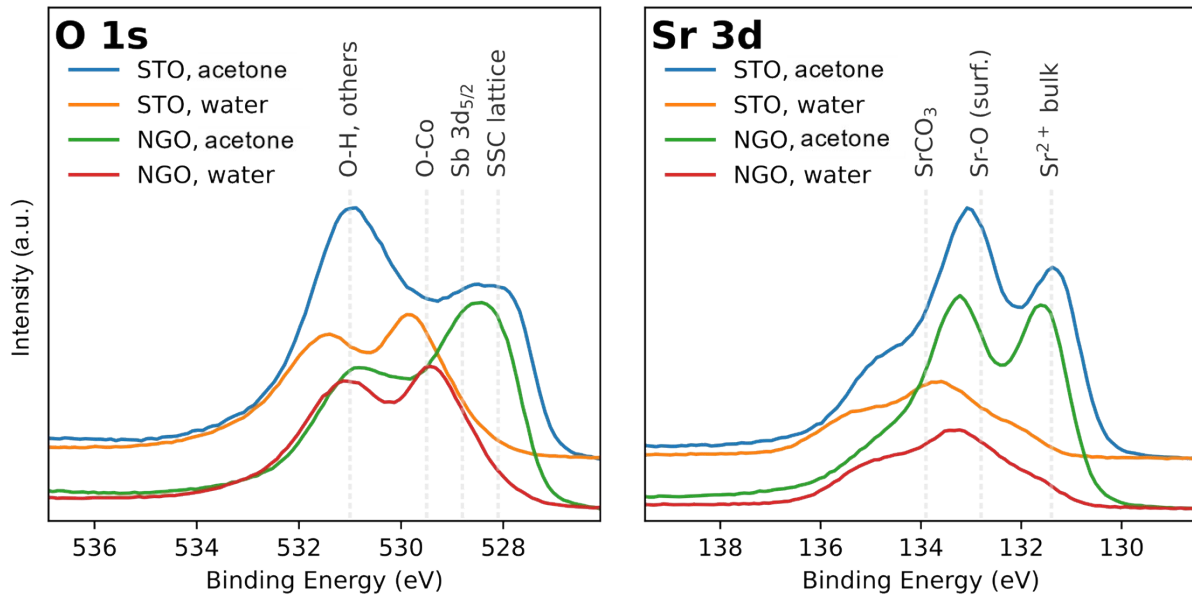


Figure S 4: Comparative XPS analysis of SCS thin film deposited by PLD on STO and NGO single crystals. Half of each sample was treated with water, the other half with acetone, both halves dried and heated in pure oxygen at 300 °C before performing the XPS analysis.

Figure S5

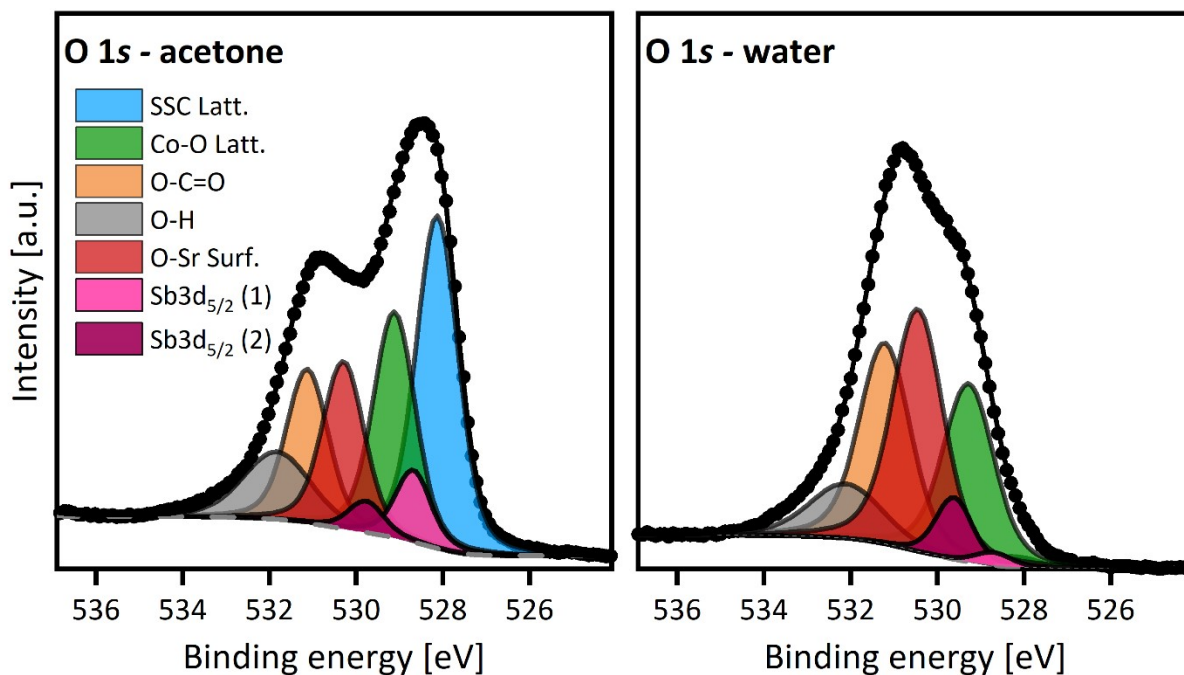


Figure S 5: Comparison of the O 1s binding energy spectra of SCS thin film. On the left the film is simply cleaned with acetone on the right instead is treated with water before being heated at 300 °C in pure oxygen. The O 1s spectra is extremely convoluted because of the many different species contributions (legend).

Figure S6

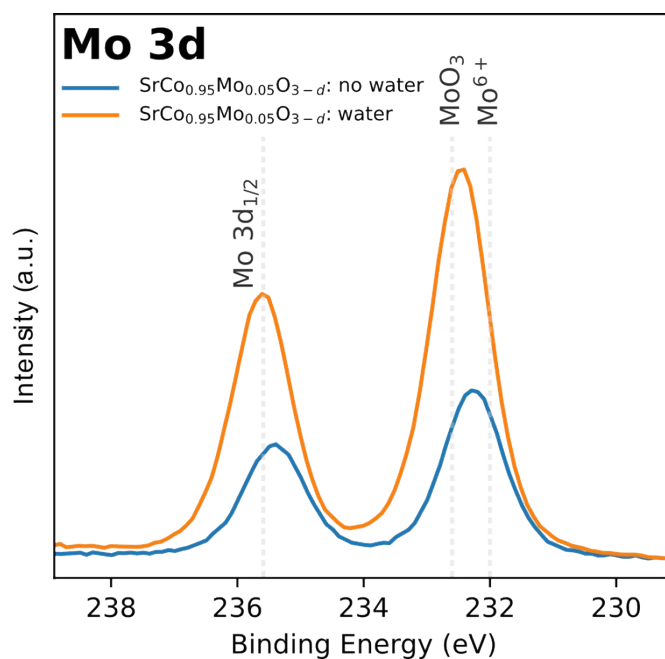


Figure S 6: XPS results comparison between as synthesized SMS powder and the same powder batch but dipped in water previous the XPS analysis. The Mo 3d binding energy for the sample treated with water moves to higher energy. This could indicate the formation of MoO₃ species suggesting the perovskite surface decomposition.

Figure S7

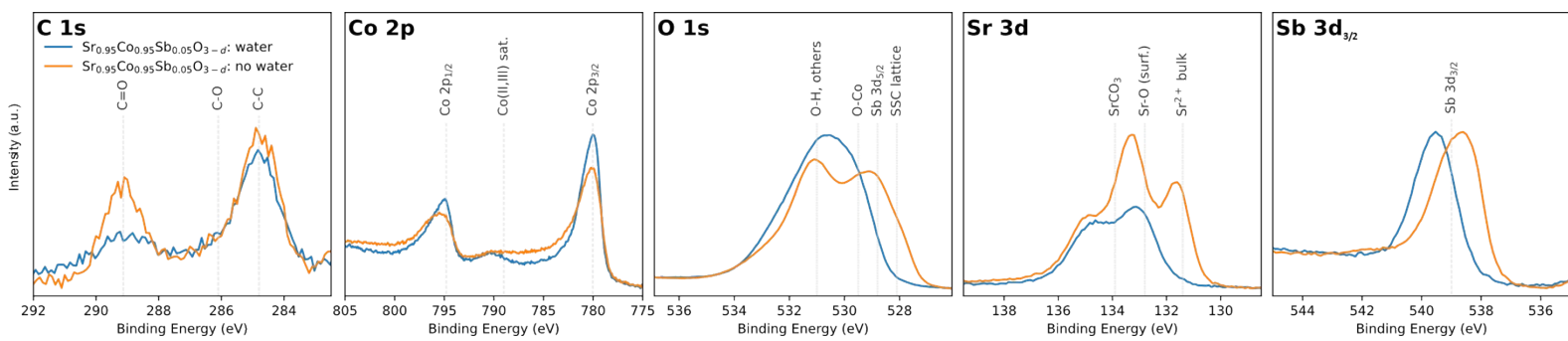


Figure S 7: Comparative XPS analysis of A-site deficient $\text{Sr}_{0.95}\text{Co}_{0.95}\text{Sb}_{0.05}\text{O}_{3-\delta}$ powder. Also, for this SCO composition, the degradation effect of water on the material surface is confirmed. In this case, the Co 2p spectra clearly indicates a decrease of the total valence of the cobalt, in agreement with the appearance at the surface of the trigonal phase.

Figure S8

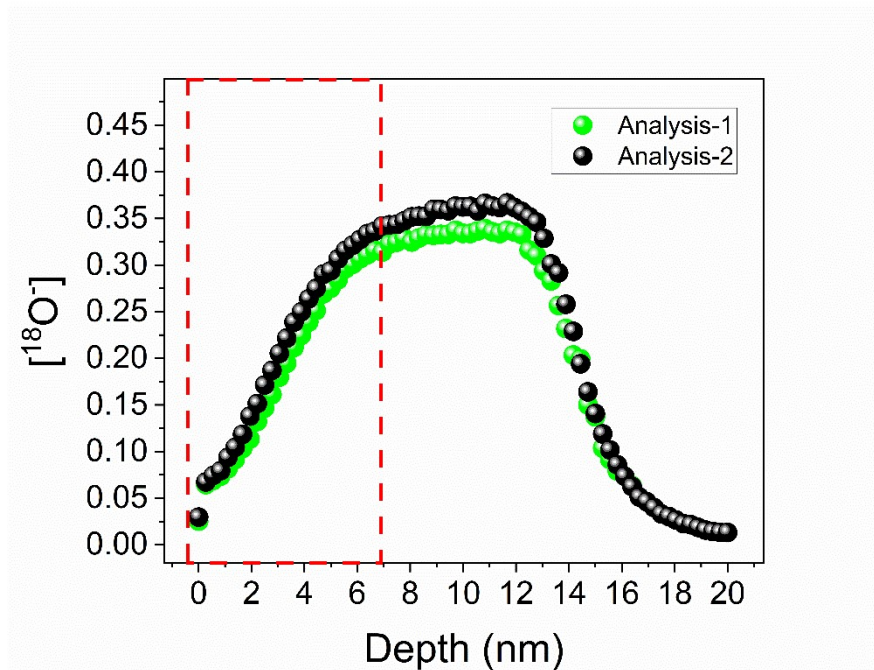


Figure S 8: Schematic explanation of the up-hill isotope exchange profile measured for an $^{18}\text{O}_2$ exchanged 15 nm SCS thin film sample. This sample was only cleaned in acetone before the exchange experiment. This uncommon $^{18}\text{O}^-$ profile measured by TOF-SIMS was interpreted as related to a partial SCS thin film surface degradation triggered by the surface reaction with the environment atmosphere humidity. Green and black dots represent two different depth profile SIMS measurements on the same sample.

Figure S9

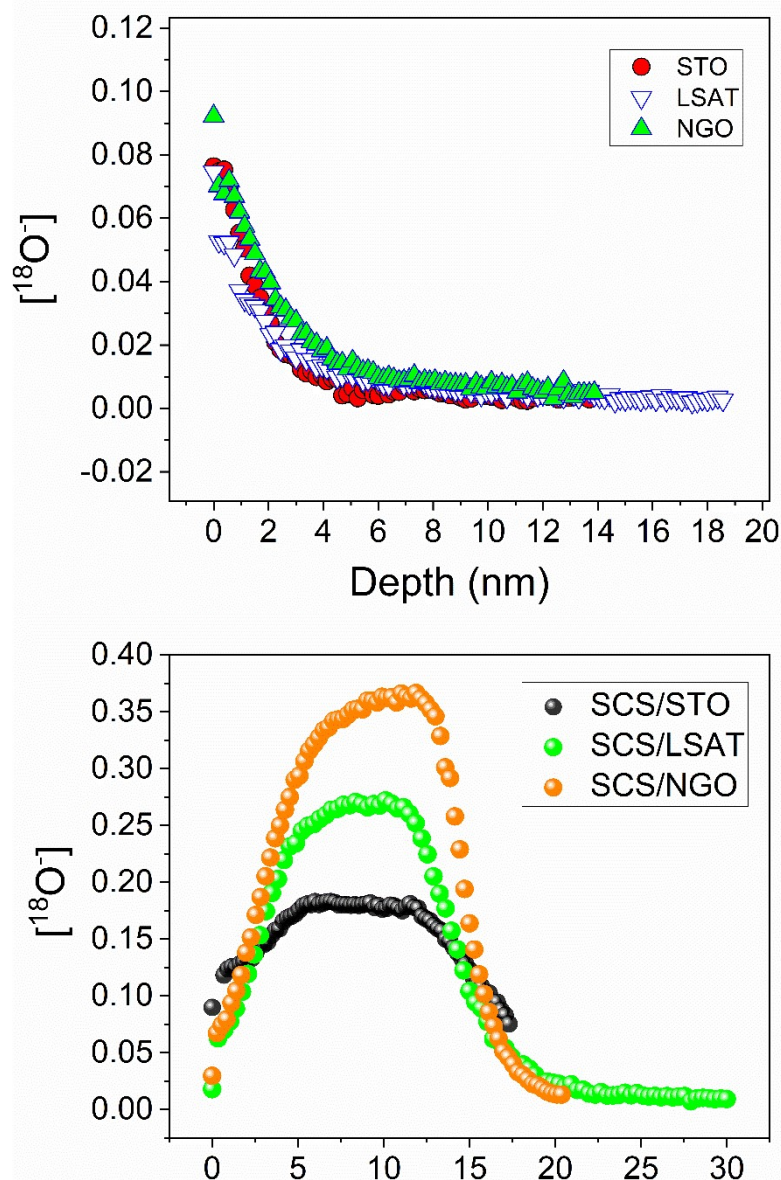


Figure S 9: Comparative IEDP analysis of 15 nm SCS thin film on STO, NGO an LSAT. Each sample was cut in half, one part cleaned in water and half in acetone before performing the exchange experiment. For each cleaning solvent, the three samples were exchanged at the same time to reduce the experimental irreproducibility. In the case of the samples cleaned in acetone a clear difference depending on the substrate employed was observed. All three samples show the initial up-hill oxygen profile. Nevertheless, a relation between the ^{18}O concentration plateau value and the SCS film in-plane strain is still matter of investigation. The sample with the higher in-plane compressive strain and consequentially with higher out-of-plane tensile strain, SCS/NGO_{SC} showed the higher ^{18}O , the one with in-plane tensile strain (higher out-of-plane compressive strain), SCS/STO_{SC} the lower.

Figure S10

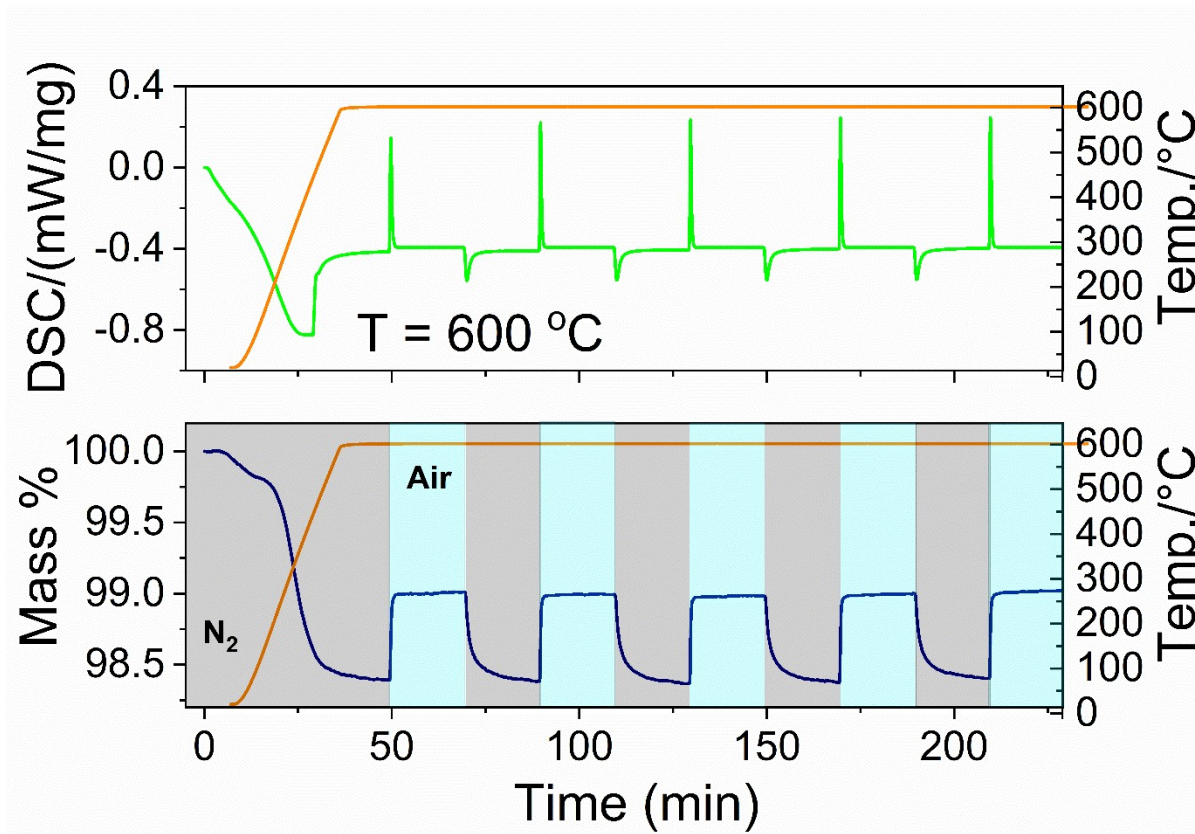


Figure S 10: TGA and DTA cycling analysis of SCS powder under reducing and oxidizing conditions alternating pure nitrogen and synthetic air respectively. Temperature was maintained constant at 600 °C.

Figure S11

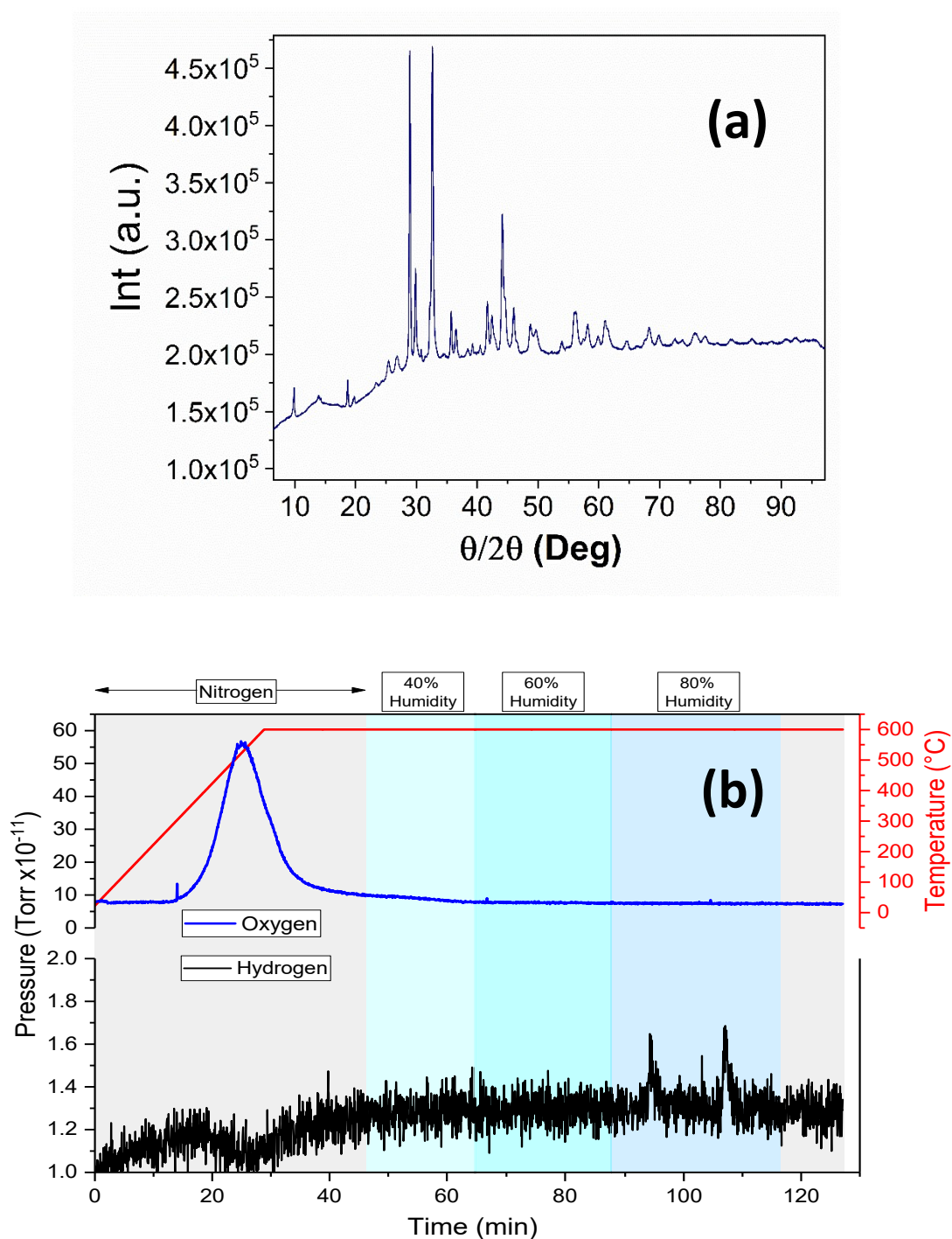


Figure S 11: XRD spectra (a) and mass spectroscopy analysis (b) of an SCS powder after isothermal ($T= 600^{\circ}\text{C}$) chemical water splitting. (a) part of the SCS phase degraded. (b) despite the oxygen evolution under low $p\text{O}_2$ conditions, very low hydrogen evolution was detected.

Figure S12

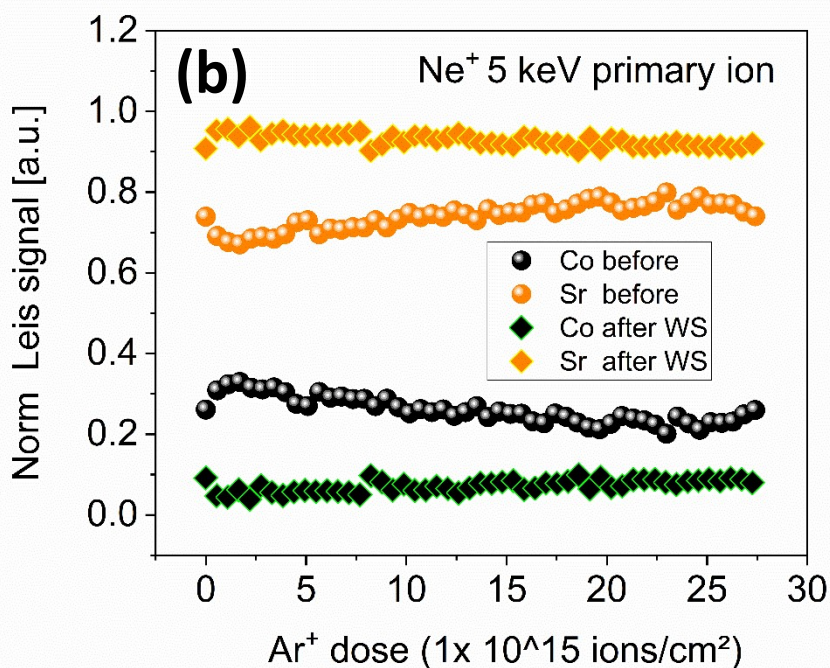
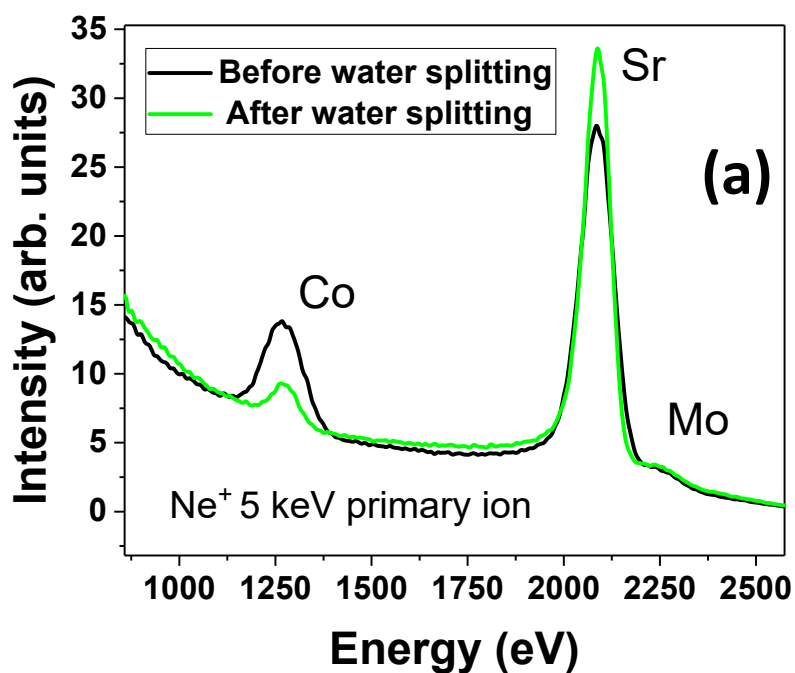


Figure S 12: LEIS (Ne⁺ 5 keV) analysis comparison of SCM powder before and after TCWS experiment. In (a) LEIS spectra of both powders surface are presented. In (b) instead, the LEIS depth profile analysis of the peak integrated area intensity in function of the total argon sputtering dose is shown.

Figure S13

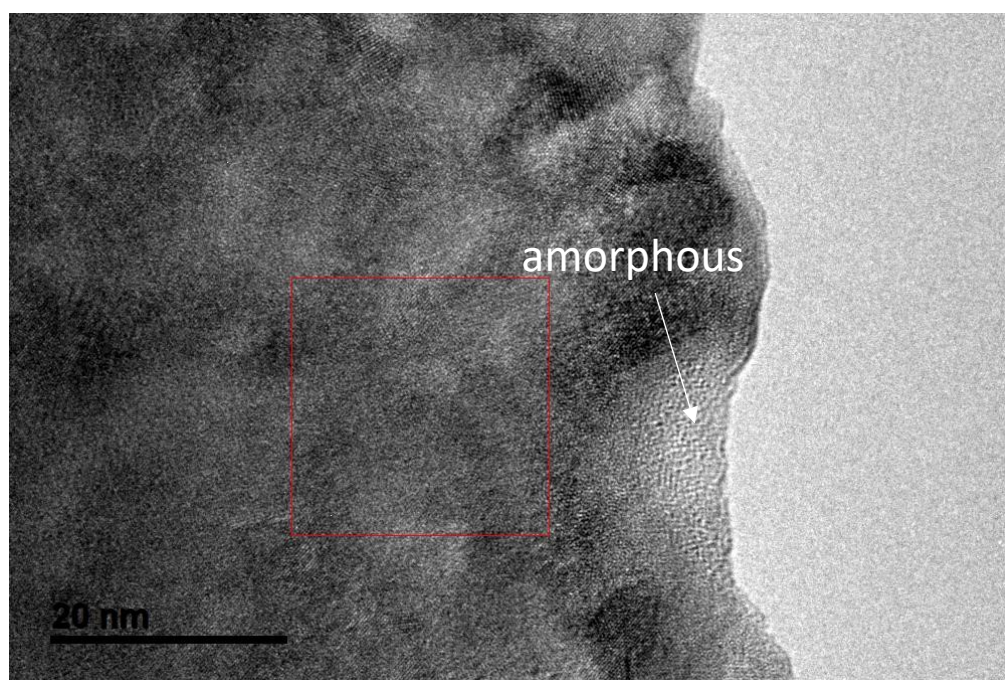
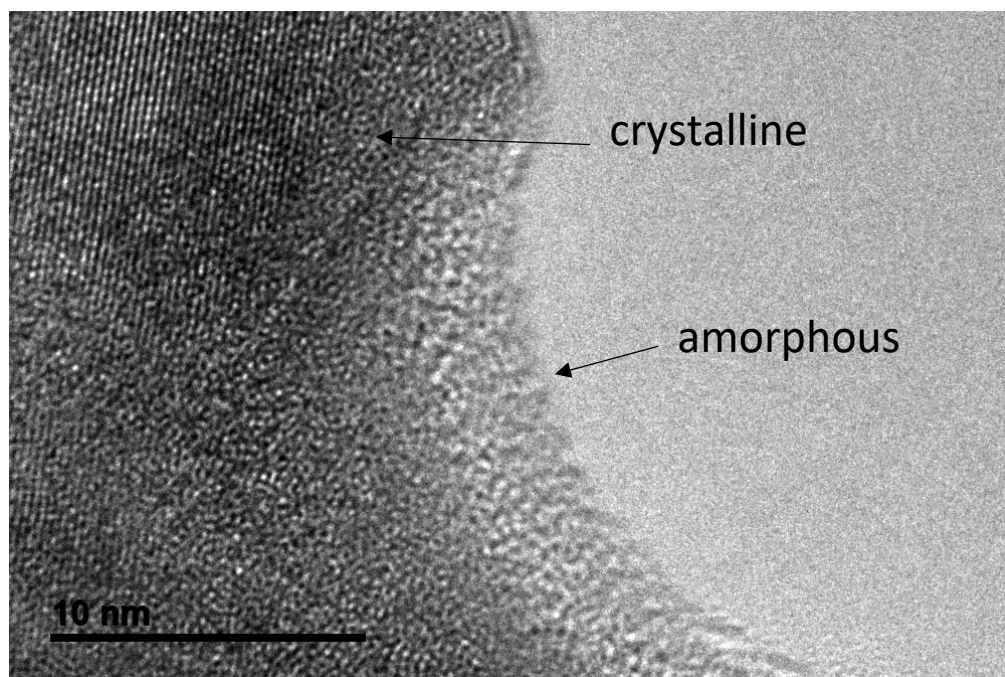


Figure S 13: HR-TEM analysis of an SSC powder treated with water at RT. Some area of the sample surface result to be amorphous.

Figure S14

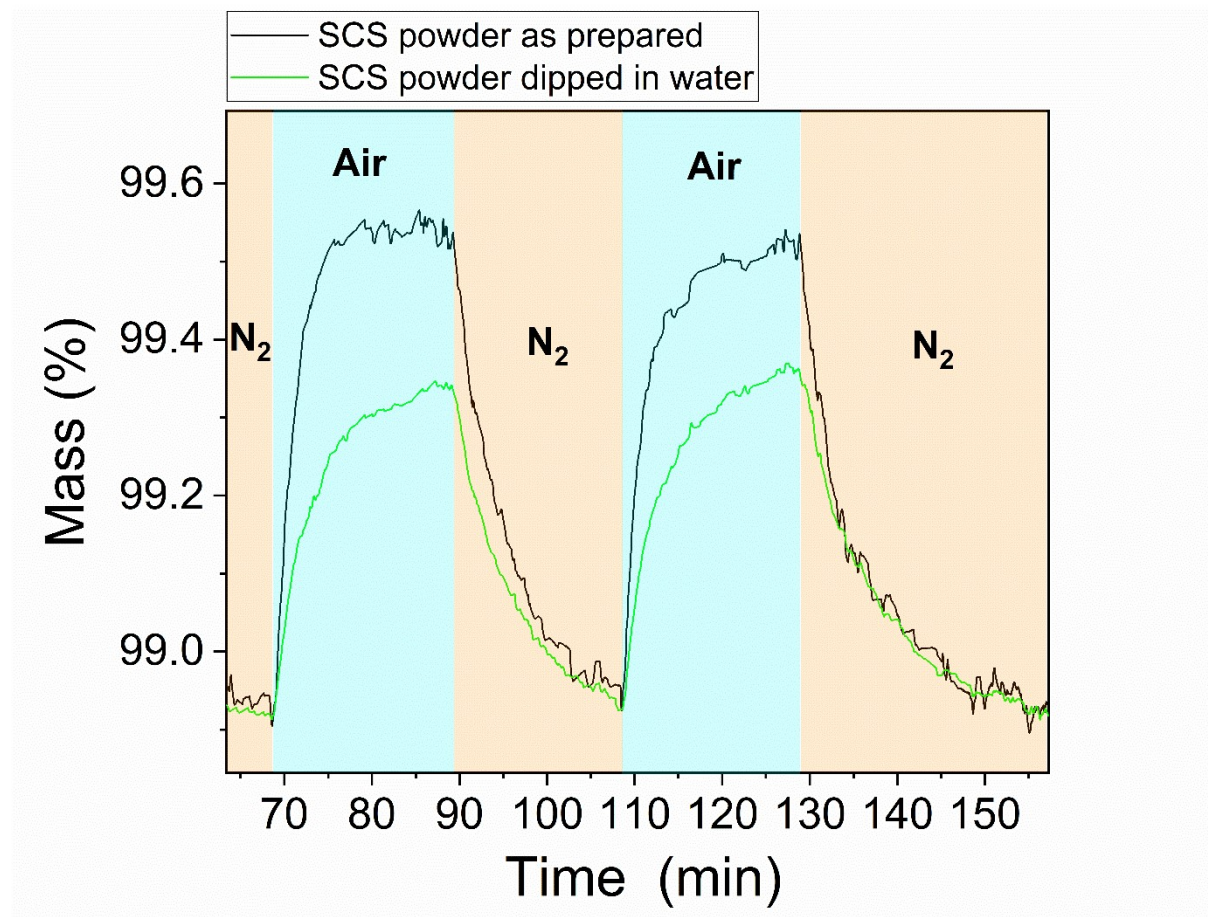


Figure S 14: TGA analysis comparison between SCS powder as synthesized and dipped in water before the TGA analysis. Note that the oxidation of the powder pre-treated in water is not completed before the start of the reduction in nitrogen.

Table S1

BE / eV	Name
528.1	SSC lattice
528.8	Sb $3d_{5/2}$
529.5	O-Co
531	O-H, others
131.4	Sr²⁺
132.8	Sr-O (surf.)
133.9	SrCO₃